NASA Technical Memorandum 87061

Burner Rig Corrosion of SiC at 1000 °C

Nathan S. Jacobson, Carl A. Stearns, and James L. Smialek
Lewis Research Center
Cleveland, Ohio

Prepared for the
Eighty-seventh Annual Meeting of the American Ceramic Society
Cincinnati, Ohio, May 5-9, 1985

NASA

BURNER RIG CORROSION OF SiC AT 1000 °C

Nathan S. Jacobson, Carl A. Stearns, and James L. Smialek
National Aeronautics and Space Administration
Lewis Research Center
Cleveland, Ohio 44135

ABSTRACT

Sintered α-SiC was examined in both oxidation and hot corrosion with a burner rig at 400 kPa (4 atm) and 1000 °C with a flow velocity of 310 ft/sec. Oxidation tests for times to 46 hr produced virtually no attack, whereas tests with 4 ppm Na produced extensive corrosion in 13-1/2 hr. Thick glassy layers composed primarily of sodium silicate formed in the salt corrosion tests. This corrosion attack caused severe pitting of the silicon carbide substrate which led to a 32 percent strength decrease below the as-received material. Parallel furnace tests of Na_2SO_4/air induced attack yielded basically similar results with some slight product composition differences. The differences are explained in terms of the continuous sulfate deposition which occurs in a burner rig.

E-2512

INTRODUCTION

Silicon carbide is being considered as a prime candidate ceramic material for hot-gas-path components in advanced combustion turbine engines. Therefore, it is essential to know how silicon carbide responds to conditions which might be encountered in the operation of such heat engines. The work reported here was undertaken to assess the high temperature environmental durability of alpha-silicon carbide (α-SiC) under conditions which are known to produce corrosive attack of superalloys in combustion turbines. The primary corrodant is molten sodium sulfate, formed by the reaction of sulfur impurities in the fuel and ingested sodium chloride. Degradation by this salt is termed "hot corrosion."

Ceramic components in heat engines are expected to operate at significantly higher temperatures than their superalloy counterparts. Therefore it has generally been assumed that sodium sulfate will not deposit and hot corrosion will not occur.[1] Higher operating temperatures can decrease the possibility of sodium sulfate deposition, especially as the dew point is approached. However high operating pressures of present and future engines raise the dew point and allow deposition to occur at higher temperatures.[2] Therefore it is not unreasonable to expect that certain regions of hot-gas-path components will be in temperature-pressure-salt concentration domains where deposition can take place and therefore the existence of molten sodium sulfate on ceramic surfaces is not precluded. Evidence has been accumulating which indicates that this molten sulfate can severely attack SiC and Si_3N_4.[3-8]

We have recently shown[6-8] in laboratory furnace tests that sodium sulfate induced corrosion degradation of α-SiC can be very severe at 1000 °C. Specimens of α-SiC were coated with thin films of Na_2SO_4 and corroded in both SO_3-O_2 and air environments. Thick glassy products, composed of silica and silicates, formed after only 1 hr. Removing these products with HF revealed that corrosion severely pitted the SiC substrate. Strength tests after 48 hr showed ~50 percent strength decrease for the Na_2SO_4/SO_3-O_2 corroded SiC and ~40 percent for the Na_2SO_4/air corroded SiC. Fractography studies proved that corrosion pits were indeed the primary sources of failure.

There is only limited information on burner rig corrosion tests of ceramics. Richerson and Yonushonis[9] showed in cyclic burner rig tests that both hot pressed and reaction bonded silicon nitride undergo a strength reduction as a result of exposure to a flame seeded with 5 ppm sea salt. Schlichting[10] has also shown that silicon nitride is attacked by sodium

sulfate in a burner rig. Finally, Napier[11] has very recently reported engine test results for reaction bonded silicon carbide tested at 960 °C with 3 ppm sea salt. While it is not clear if deposition did or would be expected to occur, numerous failures of silicon carbide were observed after 25 hr of testing.

In the present study, SiC was examined in a burner rig under accurately controlled conditions. This enabled selection of parameters to allow deposition of sodium sulfate in all runs. Tests were run at 1000 °C--a temperature at which furnace tests show rapid kinetics.[8] After a run, product morphology and composition were determined. In addition, the strength of the corroded specimens was determined and compared to that of the as-received specimens.

Burner and furnace tests have both been used to study the hot corrosion of superalloys.[12] Burner rigs more closely model the situation encountered in a gas turbine. However it is difficult to control the various test parameters, as can be precisely done in a furnace. Due to this fact, there may be a disparity between these two types of tests for superalloys.[12] Hot corrosion studies of ceramics are relatively recent, so parallel furnace studies were performed to assess the differences and similarities between burner and furnace hot corrosion tests of ceramics.

Experimental

The material studied was commercially available sintered α-SiC.* This material has high strength retention at elevated temperatures and shows particular promise for future applications.[13] Samples were cut to approximately 2.5 by 0.5 by 0.25 cm and ground to a 15 μm finish with diamond.

---

*Carborundum Hexaloy, Ca. 1977, Niagara Falls, N.Y.

As mentioned, it is essential to understand the factors which control deposition before initiating burner corrosion tests. Liquid sodium sulfate forms from the reaction of the vapor species:

$$2NaCl(g) + SO_2(g) + \frac{1}{2} O_2(g) + H_2O(g) \rightarrow Na_2SO_4(\ell) + 2HCl(g) \qquad (1)$$

The dew point is the highest temperature at which condensed phase sodium sulfate can form and was calculated from the NASA CEC program.[14] This computer program calculates chemical equilibrium information by minimizing free energies. Table I lists the dew point for a realistic range of added sodium (as sodium chloride) and 0.05 weight percent sulfur in the fuel (Jet A). The concentration of sodium is defined here with respect to the air flow rate. A fuel to air ratio of 0.025 was used since this gave a sample temperature near 1000 °C. Table I lists dew points at both 100 and 400 kPa (1 and 4 atm). Note that 400 kPa (4 atm) raises the dew point 60 to 70 °C and is necessary to obtain deposition above 1000 °C for sodium concentrations equal to or greater than 1 ppm.

Thus testing at high pressures is important for several reasons. First it more accurately models the conditions inside the engine. Second it raises the dew point to 1000 °C or greater with the appropriate sodium concentration. Laboratory studies on SiC indicate important corrosion effects occur at this temperature. It should also be noted that higher pressures increase the Na_2SO_4 deposition rate,[2] which may lead to more severe corrosion. For example, a 400 kPa (4 atm) 4 ppm Na burner exposure deposits Na_2SO_4 on samples at 960 °C ten times faster than a comparable exposure at 100 kPa (1 atm).[15,16]

All burner rig testing was carried out in the apparatus shown schematically in Fig. 1. This apparatus could accommodate testing at pressures up to 400 kPa (4 atm). Burner rig oxidation (without NaCl) and

corrosion (with NaCl) tests were run at a fuel to air ratio of 0.025±0.002 which yielded a sample temperature of 990±10 °C. Most corrosion tests were done with 4 ppm sodium, however a few were done with 1 ppm sodium. The sodium was added to the flame by air aspirating a sodium chloride solution into the combustor. The gas flow velocity over the test sample was 310±10 ft/sec. For some runs, various numbers of cycles, intentionally or inadvertently, occurred in the testing. A cycle was when the burner turned off and the sample temperature and system pressure decreased to ambient. In the corrosion tests, reheating of the sample to test temperature was always done in the oxidation mode, i.e., without salt added to the burner. One-half hr at temperature in the oxidation mode always preceded corrosion mode testing. No effect of cycling, for up to five cycles, was noted in either oxidation or corrosion of the α-SiC samples.

Samples were supported in grade A lava (aluminum silicate) holders. The samples had their length perpendicular to the flow and their thickness facing the flow. Initial experiments were done with a nickel base alloy (RA 330) test section. Under these conditions, the alloy test section severely corroded and deposited various transition metals on the SiC samples (Table II). Therefore the alloy test section was replaced with an alumina tube, which gave substantially cleaner corrosion products (Table II). Despite the impurities in the first set of specimens, the corrosion products had similar sodium and silicon quantities and morphologies as the set run with an alumina liner.

In order to characterize similarities and differences between burner and furnace tests, sintered α-SiC was also corroded in a laboratory furnace. Samples were coated with 2 to 3 mg Na_2SO_4/cm^2 and placed in a tube furnace at 1000 °C with a flowing air atmosphere. It will be shown that this

atmosphere comes close to duplicating the situation encountered in the burner rig.

Corroded specimens from both tests were analyzed with conventional methods. Product morphologies were determined from both optical and scanning electron microscopy (SEM). The corrosion products were easily removed by a 10 percent HF solution, allowing examination of the SiC substrate. In addition, the amounts of Na, Si, and $SO_4^=$ in the HF solution were determined by chemical analysis.[6] This gave the amount of Na_2O, SiO_2, and Na_2SO_4 in the glassy products. Corroded specimens were also sputter coated with a layer of gold and copper plated. Mounting and polishing to 1 μm gave a cross section for electron microprobe examination.

For strength tests, the large lumps of glassy corrosion product on the specimens had to be removed by polishing to permit accurate alignment in the four point bend test fixture. This was done first with SiC papers and then 15 μm diamond. The modulus of rupture was measured in a four point bend fixture with an outer span of 1.9 cm and an inner span of 0.95 cm and a loading rate of 0.05 cm/min. The bend strengths were calculated based on the original specimen dimensions to give a true measure of the retained load carrying capability. However the final specimen thickness due to surface recession and post-corrosion polishing was only reduced ~20 μm, which would cause only a 2 percent change in the calculated strengths. Fracture origins of the corroded specimens were identified with the SEM.

RESULTS AND DISCUSSION

Figure 2 shows two specimens--one oxidized for 46 hr in a burner with no salt added, and one treated for just 13-1/2 hr in the same rig with 4 ppm salt injected. The oxidized sample shows essentially no corrosion attack and looks very similar to the as-received samples. However the sample exposed in a salt containing environment shows a thick product with considerable corrosion

evident. Much of this glassy product is on the trailing edge (i.e., furthest from the combuster) of the specimen. This suggests that either liquid sodium sulfate or the liquid glassy products are blown to the rear of the specimen by the high gas velocities.

Figure 3 is a detailed view of the product layer. Portions of this product were chipped from this specimen mechanically to examine the interior of the layer. Figure 3(b) is a region close to the product/carbide interface and Fig. 3(c) is the underside of a portion of spalled product. Note the extensive bubble formation--indicating that the corrosion reactions generate locally large gas pressures. These bubbles created a delicate product structure, which could spall easily.

Figure 4 is a polished cross section of these products. Elemental mapping revealed a uniform distribution of silicon, oxygen, and sodium. Most of the sulfur is at background levels, except for a few concentrated regions. These results suggest that the scale is composed primarily of $Na_2O \cdot x(SiO_2)$ and a few regions of Na_2SO_4. X-ray diffraction of the scale did not identify any crystalline products.

Chemical analysis revealed further information about the composition of the products. These products were essentially insoluble in water, however they readily dissolved in a 10 percent HF solution. Sodium silicate should dissolve in water and HF, silica should dissolve in HF only. SEM/energy dispersive spectra analyses of the corrosion products indicated that the relative level of the sodium decreased from ~5 percent of the silicon peak to ~1 percent of the silicon peak after 2 hr in warm water. No discernable morphological changes were obtained despite the apparent slight dissolution of sodium silicate. Thus it is likely that the sodium silicate is trapped in a silica matrix. This explains why the products were only soluble in HF, despite the elemental maps (Fig. 4) which showed primarily sodium silicate.

The HF solution was analyzed for sulfate anion, sodium, and silicon. From these quantities, the amounts of Na_2SO_4, Na_2O, and SiO_2 were calculated.[6] These results are shown in Table III. Note there is only a small amount of Na_2SO_4 and a larger amount of Na_2O. Apparently after Na_2SO_4 deposits, it decomposes to Na_2O. Using the appropriate stoichiometric relationships, a deposition rate of 0.63 mg Na_2SO_4/cm^2-hr is calculated for position 1. This shows reasonable agreement with a rate of ~2.2 mg Na_2SO_4/cm^2-hr estimated from deposition theory.[15,16] Table III also shows a difference in the amount of sodium deposited on samples in positions 1 and 2. It may be that some sodium sulfate deposits on the walls in between the two samples or that the flame does not fully recover after impinging on the first specimen. Nonethless, deposition and hot corrosion occurred on both specimens.

Table III also presents the large quantities of SiO_2 formed in hot corrosion as compared to oxidation which gives only ~0.5 mg SiO_2/cm^2 at 1000 °C.[6] Note also that the ratio of SiO_2 to Na_2O is ~4 to 5, which is near the liquidus in the Na_2O-SiO_2 phase diagram[8,17]. This position in the phase diagram indicates that the products should be primarily liquid sodium silicate, with a small amount of pure silica. This is consistent with the cross section and elemental maps (Fig. 4).

As mentioned previously, sintered α-SiC contains ~3 percent excess carbon. In furnace tests using Na_2SO_4 with a 0.01 percent SO_3/O_2 atmosphere; SiC with excess carbon corroded dramatically, whereas SiC without excess carbon did not corrode. However in furnace tests using Na_2SO_4 with an air atmosphere, SiC with and without excess carbon corroded. In order to determine the effect of excess carbon in the burner, some hot-pressed (alumina

containing) SiC[†] was examined. Chemical analysis results are presented in Table III. These are very similar to the product compositions obtained for sintered α-SiC. Furthermore the morphologies of the corrosion products on both hot-pressed and sintered α-SiC were very similar. This information suggests that burner corrosion of SiC is not very sensitive to the particular additive used in the ceramic. Thus burner experiments show similar behavior to Na_2SO_4/air furnace experiments.

The preceding observations and results can be used to derive a corrosion mechanism. It has been shown in furnace tests,[6,8] that corrosion often occurs by repeated oxidation and dissolution:

$$SiC + \frac{3}{2} O_2 \rightarrow SiO_2 + CO\uparrow \quad (2)$$

$$SiO_2 + Na_2SO_4 \rightarrow Na_2SiO_3 + SO_3\uparrow \quad (3)$$

This process very likely occurs in the burner rig. The released CO and SO_3 very likely forms the bubbles shown in Fig. 3. The sodium silicate observed in the cross section and in chemical analysis probably forms by reaction (3). It should be noted that reaction (3) is not thermodynamically favorable. However the high gas velocity in the rig removes SO_3 as rapidly as it is formed, which drives reaction (3) to the right. In a burner rig, sodium sulfate is continuously deposited. This means that reactions (2) and (3) could continue until large amounts of the SiC are consumed.

Removing the products by HF dissolution revealed a dramatic pitting attack of the SiC substrate. A view of the entire width of the corroded bar is shown in Fig. 5(a). Note the difference between the leading edge (closest to combustor) and trailing edge (furthest from combuster). The leading edge (Fig. 5(b)) exhibits deep 100 μm wide pits but only a small amount of overall

---

[†]NC 203, Norton Co., Worcestor, Ma.

surface recession (<5 μm). The corrosion products on this part of the sample were thin due to the sweeping effect of the high velocity gas stream (Fig. 2). The trailing edge in Fig. 5(c) shows more uniform and smaller 10 to 20 μm pits, but substantial overall surface recession (~20 μm). This is presumably due to the greater amount of $Na_2O \cdot x(SiO_2)$ products present here (Fig. 2) which suggests more corrosion.

These surface pits led to a substantial strength reduction in the corroded specimens relative to the as-received specimens. These results are shown in Fig. 6 and Table IV for nine burner rig specimens. The average strength value was 278 MPa or a strength decrease of 32 percent below the as-received material.[7] No significant difference was found between specimens run with the metal liner and specimens run with the alumina liner, as shown in Fig. 6, indicating that the cation impurities did not significantly affect the corrosive properties of the Na_2SO_4 deposits.

As with most studies of comparative strengths of ceramic materials, a statistical analysis of the data is imperative to make meaningful conclusions. The 95 percent confidence interval for as-received and corroded specimens is shown in Table IV. This interval for the corroded specimens is below that of the as-received specimens. Furthermore the 95 percent confidence interval for strength reduction, $\Delta\sigma_f$, do not overlap with zero which indicates that significant reductions occurred according to the Student's t-test.

Fracture origins were identified for several corroded specimens. This is shown in Figs. 7 and 8. Both figures indicate that the fracture origin existing at the center of the radial crack lines is a corrosion pit filled with a glass corrosion product. Removal of the corrosion product by HF dissolution revealed the nature of the pitting attack, shown in Figs. 7(c) and 8(c). Figure 7 is an origin for fracture initiated on the leading edge of

the specimen, where the pits were quite deep. Figure 8 is an origin for fracture initiated on the trailing edge, where the pits were shallower but overall surface recession was greater.

To further illustrate the control of fracture strength by these corrosion pits, the fracture stress was plotted as a function of pit dimensions in Fig. 9. According to the approximation of Bansal,[13] the relationship of fracture stress to elliptical crack size is given by:

$$(\sigma_f \pm 5 \text{ percent}) \approx \frac{1.68}{Y} \frac{K_{IC}}{A^{1/4}} \tag{4}$$

Here Y is a geometrical parameter, approximately equal to 2.0 for surface flaws; K_{IC} is the fracture toughness; and A is the flaw area given by $\pi ac/2$.[17] Thus for semi-elliptical surface flaws having depth a and width $2c$, equation (4) becomes:

$$\sigma_f \approx 0.75 \frac{K_{IC}}{(ac)^{1/4}} \tag{5}$$

The line in Fig. 9 is for such a relationship, with $K_{IC} = (2.79 \pm 0.17)$ MPa$\cdot$m$^{1/2}$, obtained by the chevron notch technique.[19] This is close to other K_{IC} values obtained for this material.[7] The individual data points were obtained from the pit dimensions at the fracture origins. These data cluster about the line and yield an average $K_{IC} = (3.30 \pm 0.72)$ MPa$\cdot$m$^{1/2}$, which is not statistically different from the chevron notch K_{IC} value.[19] This behavior is similar to that found in an earlier study of the fracture origins due to salt-film furnace corrosion of α-SiC.[7] The scatter in the data is due to interactions between other pits, the irregular shapes of the pits, and pits that were not associated with atomically sharp cracks.

The major observations about burner rig corrosion of SiC can be summarized as follows. The corrosion products consist of thick, glassy layers of $Na_2O \cdot x(SiO_2)$ which contain numerous trapped bubbles. These products

very likely form as a result of repeated oxidation and dissolution. Furthermore this process does not seem to be a function of any particular additive in the ceramic. Corrosion causes severe pitting of the SiC substrate. These pits were typically fracture origins and led to a 32 percent strength decrease over as-received SiC.

The preceding burner rig observations are very close to laboratory furnace results for α-SiC coated with Na_2SO_4 and corroded in a flowing air environment at 1000 °C.[6] After 13-1/2 hr, under these conditions, thick glassy products form, which contain many trapped bubbles (Fig. 10). Chemical compositions of these layers (Table III) show less Na_2O and SiO_2 than the burner rig. In addition the SiO_2 to Na_2O ratio is greater in the furnace case. A SiO_2 to Na_2O ratio of 6.2 is well within the two phase region of the Na_2O-SiO_2 phase diagram.[8,17] This indicates the products should contain a substantial amount of pure silica and sodium silicate. Indeed, the cross section (Fig. 11) of the furnace specimen shows a layer of pure SiO_2 needles on the SiC substrate. This does not occur in the burner rig case (Fig. 4). These differences can be explained by the continuous deposition in the burner rig case versus the one time deposition in the furnace case. Continuous deposition of Na_2SO_4 gives the larger amount of Na_2O and allows the oxidation-dissolution process to continue indefinitely, which gives a very thick sodium silicate scale. In the furnace tests, mechanism studies have established that once all the sodium sulfate has been consumed, pure silica grows on the carbide.[8] This layer of silica eventually stops the reaction.

Figure 12 is a surface view of the furnace corroded SiC specimen after removal of the products by HF. As in the burner case, extensive pitting occurs. As expected pitting in the furnace case is much more uniform than in the burner case. Nonetheless, after 48 hr, furnace corrosion causes a

38 percent strength decrease over the as received material (Fig. 6). A statistical treatment in Table IV shows that this is essentially the same as the strength decrease caused by burner rig corrosion. The plot of fracture stress versus pit depth (Fig. 9) also includes some Na_2SO_4/air furnace corroded specimens. Note that these show essentially the same behavior as the burner rig specimens. This burner/furnace parallel indicates that the insights gained from the precisely controlled laboratory furnace experiments are very valuable in the more applied tests.

All of the burner rig tests discussed have been at 1000 °C for 13-1/2 hr with 4 ppm Na. In order to determine the effect of salt content, some samples were run with 1 ppm Na. After 13-1/2 hr, only a very small amount of glassy product was observed. However after 40 hr, a thick glass layer, similar to that in Fig. 2(b) was observed.

CONCLUSIONS

High pressure burner rig testing has been used to examine the corrosion of sintered α-SiC. High pressures, temperatures, and gas velocities in a burner provide a more accurate model of a future ceramic engine.

Conditions were carefully chosen to allow sodium sulfate deposition. Most tests were run at 4 atm, 1000 °C and for 13-1/2 hr. Jet A fuel (0.05 percent sulfur) was used with 4 ppm sodium aspirated into the combuster. Under these conditions, severe corrosion of SiC occurred. Thick glassy layers of $Na_2O{\cdot}x(SiO_2)$ formed on the carbide surface--very likely by repeated oxidation and dissolution. Removing the glassy products with HF revealed a severe pitting of the SiC caused by the corrosion process. These pits were typically failure origins and led to a 32 percent strength decrease below that of the as-received material.

Parallel furnace tests were performed by spray coating ~2.5 mg Na_2SO_4/cm^2 on SiC samples. These were placed in a furnace at 1000 °C

for 13-1/2 hr. Morphologies of the corrosion products were very similar to those obtained from the burner rig. Compositional differences in products from the two types of tests were due to the continuous deposition of sodium sulfate in the burner rig versus the one-time deposition of sodium sulfate in the furnace. Furnace tests also produced pits in the SiC substrate. These pits led to a comparable strength decrease. The close burner/furnace parallel establishes the value of controlled laboratory experiments as an aid in understanding the actual corrosion process.

ACKNOWLEDGEMENT

The authors are grateful to Dr. S. Gokoglu for performing the Na_2SO_4 dew point and deposition rate calculations. Thanks are also due to Dr. G. Santoro for assistance with the burner rig.

REFERENCES

[1]S.C. Singhal, "Corrosion Resistant Structural Materials for Gas Turbines," in Proceedings of the 1974 Gas Turbine Materials in the Marine Environment Conference, ed. by J.W. Fairbanks and I. Machlin, Metals and Ceramics Information Center, Columbus, OH, pp. 311-334 (1974).

[2]D.E. Rosner, K. Seshadri, J.F. de la Mora, G.C. Fryburg, F.J. Kohl, C.A. Stearns, and G.J. Santoro, "Transport, Thermodynamic and Kinetic Aspects of Salt/ash Deposition Rates from Combustion Gases," in 10th Materials Research Symposium: Characterization of High Temperature Vapors and Gases. Vol. 2, NBS-SP-561, National Bureau of Standards, Washington, D.C., pp. 1451-1474 (1979).

[3]R.E. Tressler, M.D. Meiser, and T. Yonushonis, "Molten Salt Corrosion of SiC and Si_3N_4 Ceramics," J. Am. Ceram. Soc., 59 [5-6], 278-279 (1976).

[4]D.W. McKee, and D. Chatterji: "Corrosion of Silicon Carbide in Gases and Alkaline Melts," J. Am. Ceram. Soc., 59 [9-10] 441-444 (1976).

[5]J.R. Blachere, and F.S. Pettit, "High Temperature Corrosion of Ceramics," DOE/ER/10915/3, Feb. 1984.

[6]N.S. Jacobson, and J.L. Smialek, "Hot Corrosion of Sintered α-SiC at 1000 °C," J. Am. Ceram. Soc., (in press, 1985).

[7]J.L. Smialek, and N.S. Jacobson, "Mechanism of Strength Degradation for Hot Corrosion of SiC," (in preparation for J. Am. Ceram. Soc., 1985).

[8]N.S. Jacobson: "Kinetics and Mechanism of SiC Molten Salt Corrosion," (submitted to J. Am. Ceram. Soc., 1985).

[9]D.W. Richerson and T.M. Yonushonis, "Environmental Effects on the Strength of Silicon-Nitride Materials," in Proceedings of the DARPA/NAVSEA Ceramic Gas Turbine Demonstration Engine Program Review, MCIC-78-36, Metals and Ceramics Information Center, Columbus, OH, 1977, pp. 247-271, (1977).

[10]J. Schlichting, "Oxidation and Hot Corrosion Behaviour of Si_3N_4 and SiAON," in Nitrogen Ceramics, ed. by F.L. Riley, Noordhoff, Leyden, pp. 627-634 (1977).

[11]J.C. Napier, "Manufacturing Methods for Ceramic Nozzle Section for Gas Powered APU'S," Solar Turbines Inc. Report SR84-R-4692-64, May 1984.

[12]P. Hancock, "The Use of Laboratory and Rig Tests to Simulate Gas Turbine Corrosion Problems," Corr. Sci., 22, [1] 51-65 (1982).

[13]C. Belleau, W.L. Ehlers, and F.A. Hagen, "Materials Review of Improved Automotive Gas Turbine Engines," Chrysler Corporation, NASA Cr-159673, Apr. 1978.

[14]S. Gordon, and B.J. McBride, "Computer Program for Calculation of Complex Chemical Equilibrium Compositions, Rocket Performance, Incident and Reflected Shocks, and Chapman-Jouget Detonations," NASA SP-273, 1976.

[15]D.E. Rosner, B.K. Chen, G.C. Fryburg, and F.J. Kohl, "Chemically Frozen Multicomponent Boundary Layer Theory of Salt and/or Ash Deposition Rates from Combustion Gases," Combust. Sci. Technol., 20, [3-4] 87-106 (1979).

[16]S.A. Gökoğlu, B.K. Chen, and D.E. Rosner, "Computer Program for the Calculation of Multicomponent Convective Diffusion Deposition Rates from Chemically Frozen Boundary Layer Theory," NASA CR-168329, Jan. 1984.

[17]W.D. Kingery, H.K. Bowen, and D.R. Uhlmann: Introduction to Ceramics, p. 359, Wiley, New York, 1976.

[18]G.K. Bansal, "Effect of Flaw Shape on Strength of Ceramics," J. Am. Ceram. Soc., 59 [1-2] 87-88 (1976).

[19]J.H. Wiegand, private communication, NASA Lewis Research Center, (1985).

TABLE I. - DEW POINTS (°C) FOR SODIUM SULFATE DEPOSITION

[0.05 percent sulfur in the fuel, fuel/air = 0.025, Na added as NaCl.]

Na, ppm	1×10^5 Pa, (1 atm)	4×10^5 Pa, (4 atm)
0.5	920	981
1.0	938	1001
2.0	954	1020
3.0	964	1030
4.0	970	1038

TABLE II. - CHEMICAL ANALYSIS OF CORROSION PRODUCTS-RUN IN BURNERS WITH DIFFERENT LINERS

Liner	Position	Na wt %	Si wt %	Ni, ppm	Fe, ppm	Cr, ppm	Mn, ppm
RA-330	1	13	32	59 100	23 640	4 700	1 182
	2	10	31	84 170	38 100	10 000	2 000
Al_2O_3	1	14	33	<0.05	380	<0.05	<0.05
	2	16	33	680	730	<0.05	<0.05

TABLE III. - CHEMICAL ANALYSES OF CORROSION PRODUCTS
1000°C-13.5 hr TREATMENT

[All quantities in mg/cm^2.]

Material	Test	Position	Na_2SO_4	$Na_2O \cdot x(SiO_2)$		
				Na_2O	SiO_2	x
Sintered α-SiC	Burner 13-1/2 hr 4 ppm Na	1	0.06	3.71	14.72	4.1
		2	0.28	1.63	8.50	5.4
HP-SiC	Burner 13-1/2 hr 4 ppm Na	1	0.01	3.60	15.81	4.5
		2	0.01	1.70	7.80	4.7
Sintered α-SiC	Furnace 13-1/2 hr	Average of two	0.01	0.79±0.19	4.77±0.77	6.2

TABLE IV. - STRENGTH OF Na_2SO_4 CORRODED α-SiC

	σ_f, MPa	S, MPa	n	95 percent C.I. of σ_f, MPa	$\Delta\sigma$	95 percent C.I. of $\Delta\sigma_f$, MPa	Significant reduction
As-rec'd	409	62	15	433,375	---	-------	-
Burner rig[a]	278	58	9	322,233	131	185, 77	✓
Furnace[b]	251	45	8	288,213	158	210, 106	✓

[a] 4 ppm Na, 4 atm, 1000 °C, 13.5 hr.
[b] 2-3 mg/cm^2 Na_2SO_4, 1 atm air, 1000 °C, 48 hr.

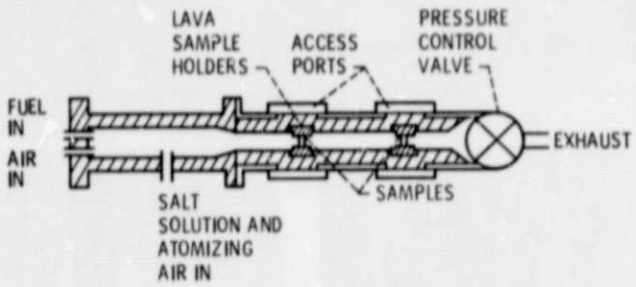

Figure 1. - Schematic of high pressure burner rig.

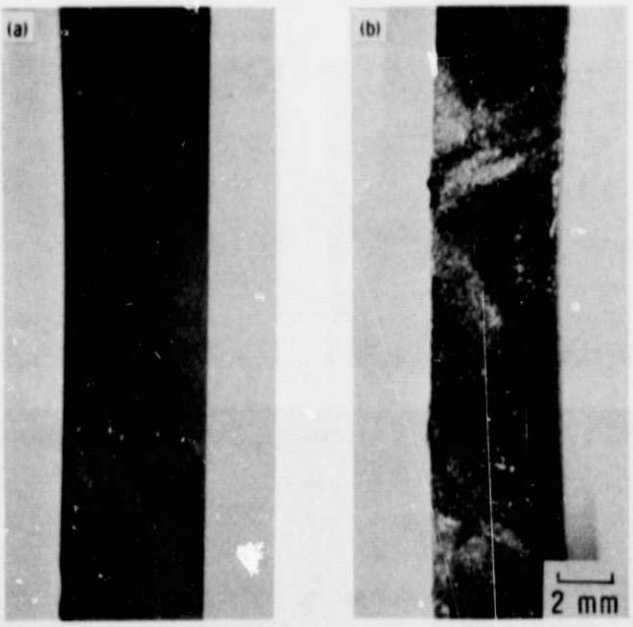

46 hr 13.5 hr

Figure 2. - Optical macrographs of sintered α-SiC treated in the burner rig. (a) For 46 hr with no Na. (b) For 13.5 hr with 4 ppm Na.

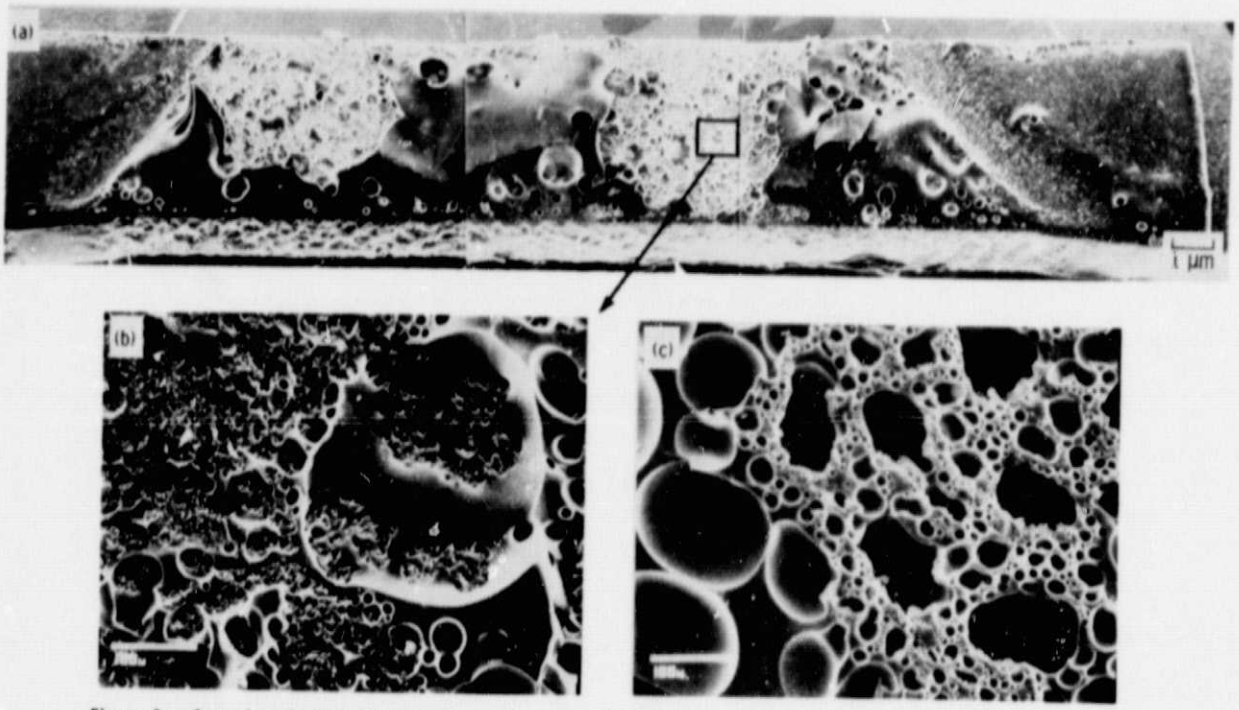

Figure 3. - Scanning electron micrographs of glassy products on burner rig sample. (a) Entire sample. (b) Enlargement of a section of products near the carbide surface. (c) Underside of a spalled section of products.

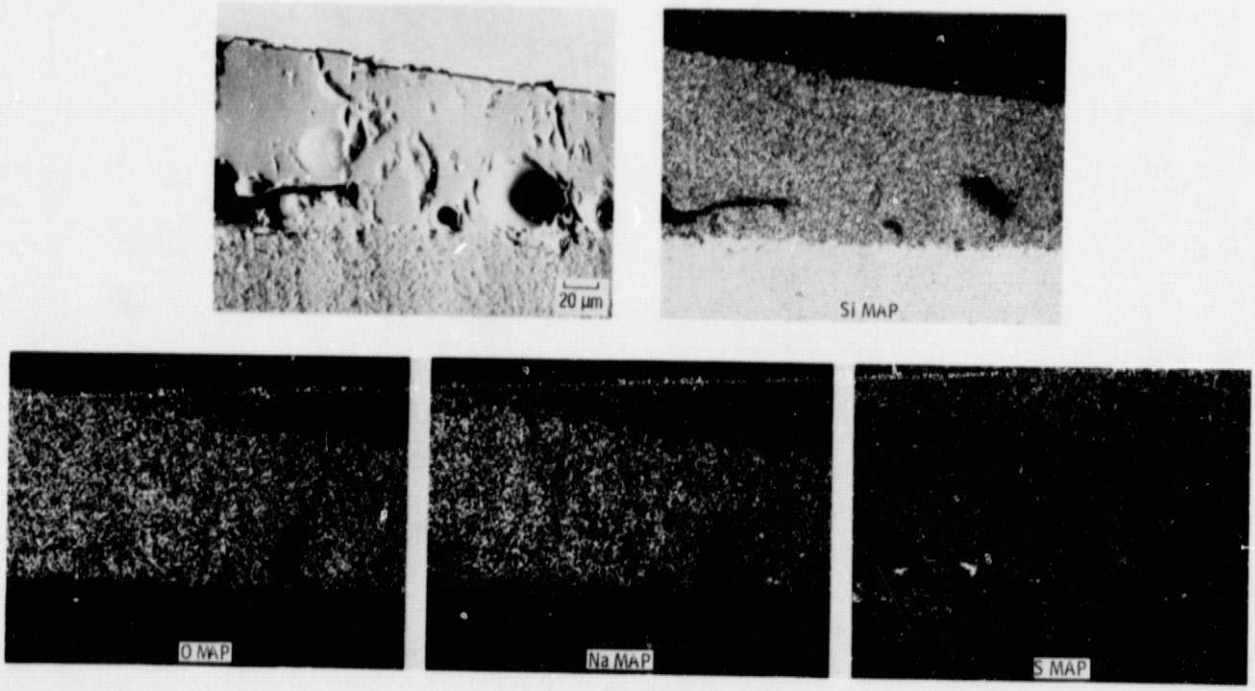

Figure 4. - Electron microprobe analysis of a polished cross section of glassy products formed by burner rig corrosion.

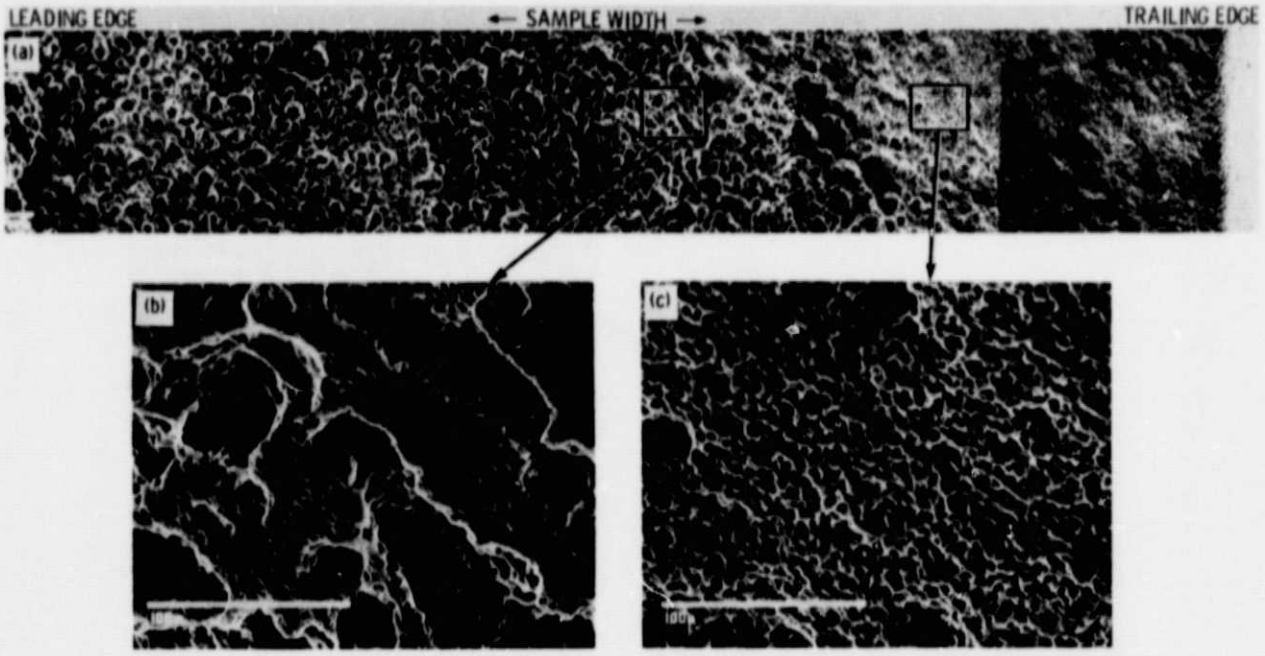

Figure 5. - Surface view of burner rig corroded SiC (products removed by HF). (a) View along entire sample width. (b) Enlargement of region typical of leading edge. (c) Enlargement of region near trailing edge.

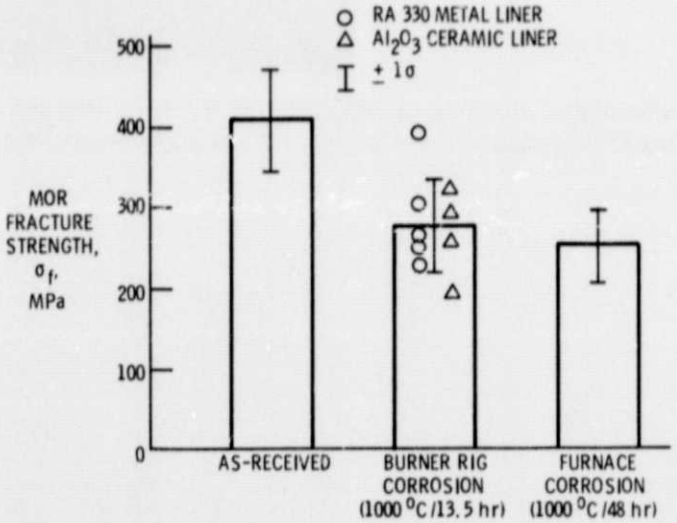

Figure 6. -Effect of corrosion on room temperature 4-pt bend of α-SiC.

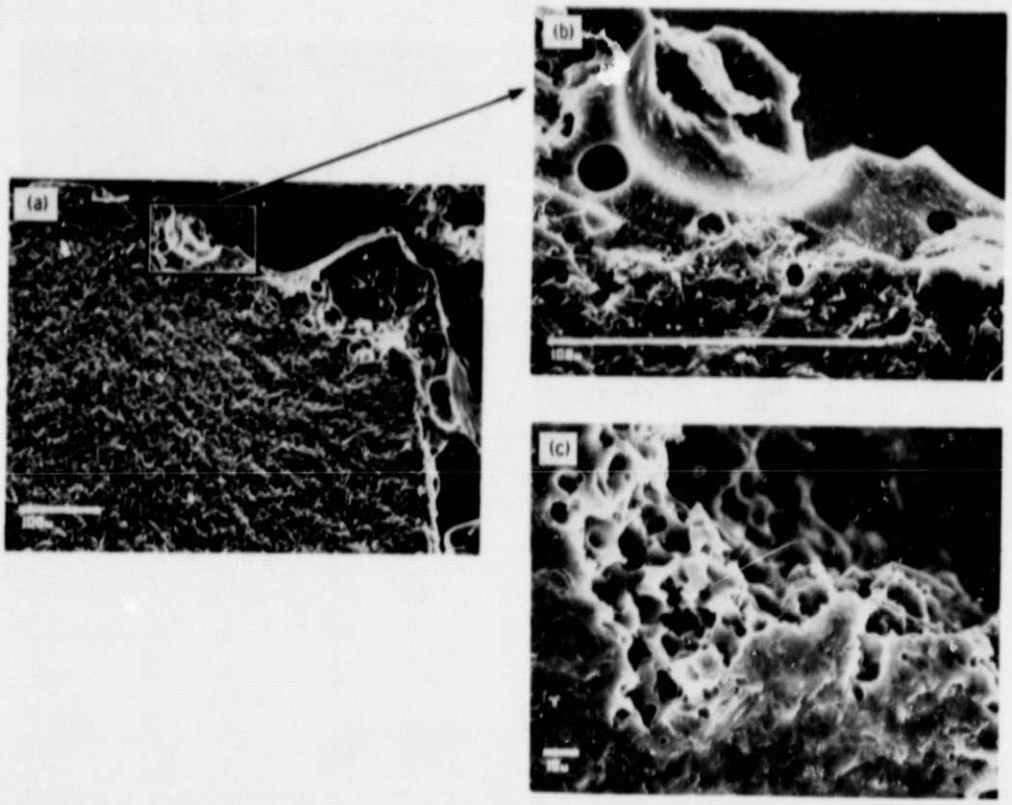

Figure 7. - Leading edge fracture origin of a burner rig corroded specimen σ_f = 304 MPa). (a) Crack lines radiating from corrosion pit. (b) Glassy product and entrapped bubbles at origin. (c) Pitting at origin revealed by HF dissolution.

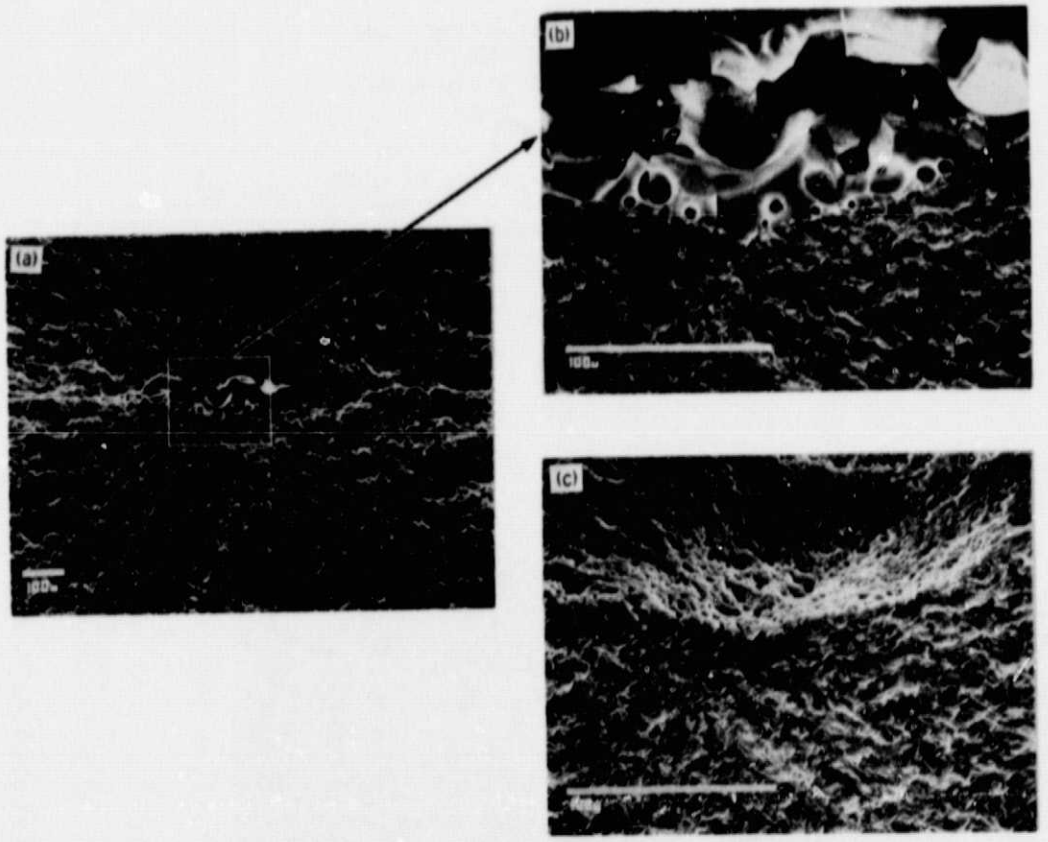

Figure 8. - Trailing edge fracture origin of a burner rig corroded specimen (σ_f 228MPa). (a) Matting halves of fracture origin. (b) Glassy product at origin. (c) Pitting at origin revealed by HF dissolution.

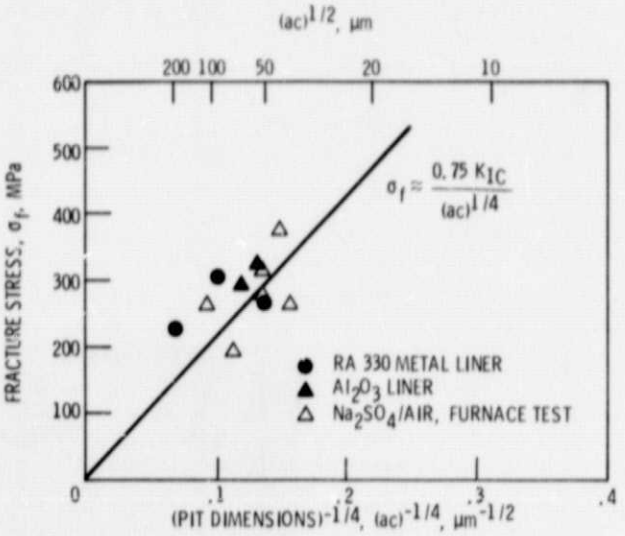

Figure 9. - Correlation of fracture stress with corrosion pit dimensions. Line predicted for $K_{IC} = 2.8$ MPa-$m^{1/2}$.

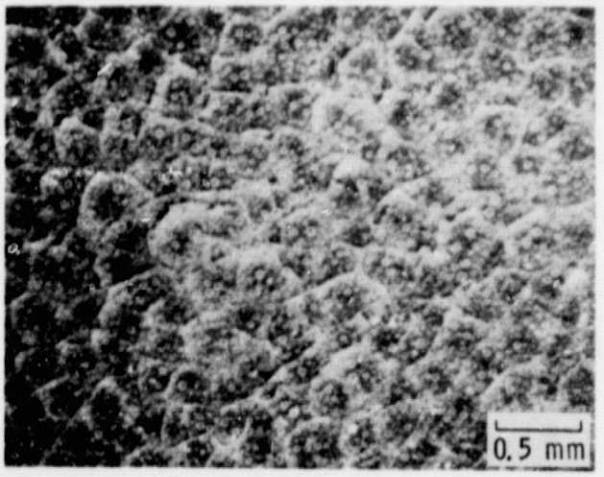

Figure 10. - Optical micrograph showing surface of furnace corroded (Na_2SO_4/air) α-SiC.

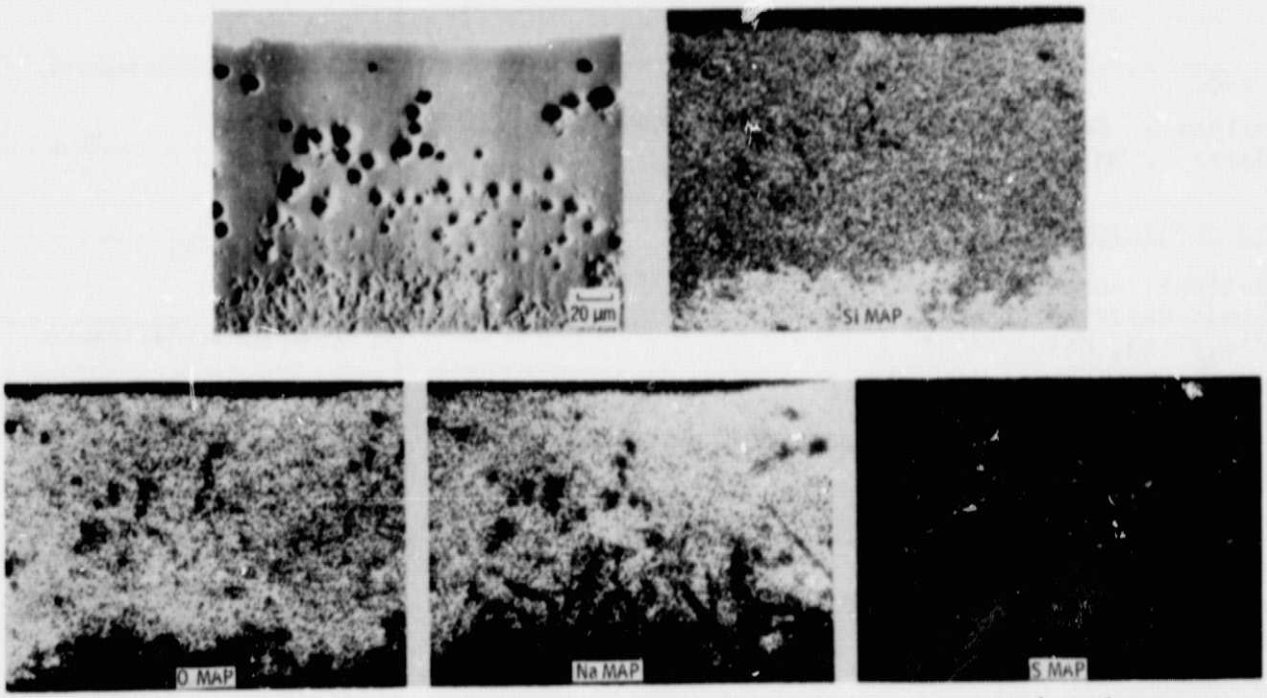

Figure 11. - Electron microprobe analysis of a polished cross section of glassy products formed on surface corroded (Na_2SO_4/air) α-SiC.

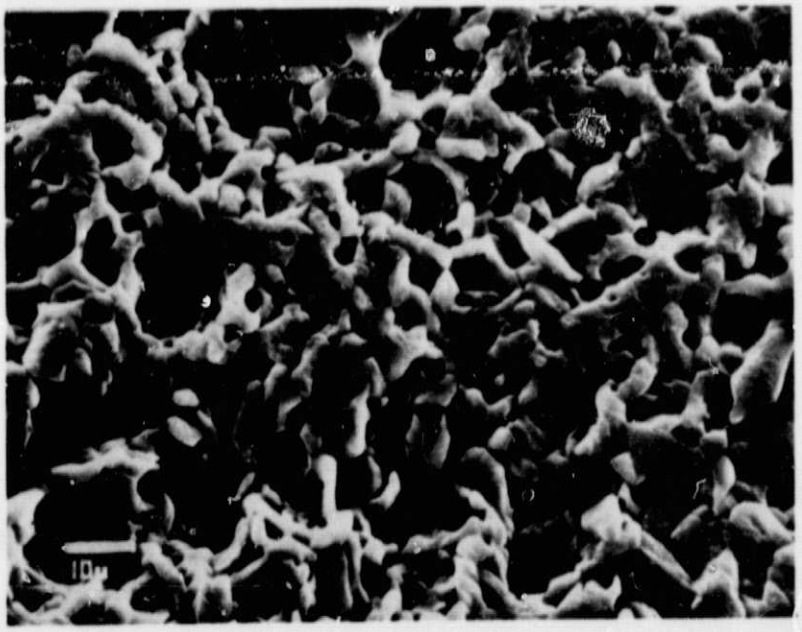

Figure 12. - Surface view of furnace corroded (Na_2SO_4/air) α- SiC (products removed with HF).

1. Report No.	2. Government Accession No.	3. Recipient's Catalog No.
NASA TM-87061		

4. Title and Subtitle	5. Report Date
Burner Rig Corrosion of SiC at 1000 °C	
	6. Performing Organization Code: 533-05-12

7. Author(s)	8. Performing Organization Report No.
Nathan S. Jacobson, Carl A. Stearns, and James L. Smialek	E-2512
	10. Work Unit No.

9. Performing Organization Name and Address	11. Contract or Grant No.
National Aeronautics and Space Administration Lewis Research Center Cleveland, Ohio 44135	
	13. Type of Report and Period Covered: Technical Memorandum
12. Sponsoring Agency Name and Address	
National Aeronautics and Space Administration Washington, D.C. 20546	14. Sponsoring Agency Code

15. Supplementary Notes

Prepared for the Eighty-seventh Annual Meeting of the American Ceramic Society, Cincinnati, Ohio, May 5-9, 1985.

16. Abstract

Sintered α-SiC was examined in both oxidation and hot corrosion with a burner rig at 400 kPa (4 atm) and 1000 °C with a flow velocity of 310 ft/sec. Oxidation tests for times to 46 hr produced virtually no attack, whereas tests with 4 ppm Na produced extensive corrosion in 13-1/2 hr. Thick glassy layers composed primarily of sodium silicate formed in the salt corrosion tests. This corrosion attack caused severe pitting of the silicon carbide substrate which led to a 32 percent strength decrease below the as-received material. Parallel furnace tests of Na_2SO_4/air induced attack yielded basically similar results with some slight product composition differences. The differences are explained in terms of the continuous sulfate deposition which occurs in a burner rig.

17. Key Words (Suggested by Author(s))	18. Distribution Statement
Corrosion; Silicon carbide; Burner rig	Unclassified - unlimited STAR Category 23

19. Security Classif. (of this report)	20. Security Classif. (of this page)	21. No. of pages	22. Price*
Unclassified	Unclassified		

*For sale by the National Technical Information Service, Springfield, Virginia 22161